Hindawi
International Journal of Optics
Volume 2019, Article ID 2987301, 13 pages
https://doi.org/10.1155/2019/2987301

Research Article

Surf Zone Mapping Using Multirotor Unmanned Aerial Vehicle Imagery

Norhalim Che Mat and Khairul Nizam Tahar

Centre of Studies for Surveying Science and Geomatics, Faculty of Architecture, Planning, and Surveying, Universiti Teknologi MARA, 40450 Shah Alam, Selangor Darul Ehsan, Malaysia

Correspondence should be addressed to Khairul Nizam Tahar; nizamtahar@gmail.com

Received 3 January 2019; Revised 22 April 2019; Accepted 2 May 2019; Published 30 May 2019

Academic Editor: E. Bernabeu

Surf zone is a sand area that stretches inside a breaking wave to limit the rise and fall of waves on the beach. Advanced technology in the geomatics field offers a fast and accurate solution to produce surf zone maps. The demand for surf zone map is increasing during the monsoon season, especially at coastal areas. Nowadays, the Unmanned Aerial Vehicle (UAV) or drone has become popular platform in the geospatial and surveying field. The aim of this study is to produce surf zone 3D surface mapping by using a multirotor Unmanned Aerial Vehicle. There are four phases in this study which are image acquisition, UAV image processing, photogrammetric results, and analysis. The image acquisition was solely obtained using a multirotor UAV based on the photogrammetric concept. The acquired UAV images were processed using commercial software with a specific workflow. Photogrammetric products such as digital elevation model, orthophoto, contour, and surf map zone were produced. The analyses of these results were conducted based on different epochs on the selected months. The accuracy for northing, easting, and height coordinates was 1.026m, 0.838m, and 0.419m, respectively. It can be concluded that the UAV was able to produce a surf zone map with reliable accuracy. This platform is very useful for fast decision making, especially during disaster incidents.

1. Introduction

Surf zone is an area that stretches between the inside of the surf and the rise and fall of waves on the beach [1]. Surf zone is the most important in the analysis of coastal processes because the high waves in the area is unstable due to the energy loss when a wave breaks; thus, high turbulence occurs, causing sediment transport processes especially during the monsoon season [2]. Beach profile changes are the phenomenon of a change in elevation of the bottom waters of the beach area if viewed by a cut perpendicular to the beach [3, 4]. Model changes in the beach profile consist of the transformation module wave, also known as wave transformation module, module sediment, and bathymetric change module [5]. Mapping the surf zone is important to observe the changes in the region and ensure that it is safe to bathe, swim, and have picnics on the beach. This is because a steep surface signifies that it is not safe for a picnic. This study coincides with the statement that an area with a high percentage of slope has a high erosion rate [6]. Nowadays, geographic information system (GIS) applications are very helpful in providing, analyzing, and displaying any geospatial data, including the mapping of surf zone. The use of geographic information system to provide a complete surf zone map with land data profile, size, shape, and texture is a smart move and saves time and manpower since mapping is done in digital form. Wave consists of wavelength, wave height, wave period, wave steepness, and frequency of the wave. Wavelength is the distance between two consecutive peaks or two valleys. Wave height is the vertical distance between the peaks and troughs and wave period is the time it takes the wave to return to the original point. The slope of the wave is high and a comparison is made between multiple wavelengths. Wave frequency is the number of waves that occur in a time unit [7, 8].

In fact, the waves formed by the wind would spread farther from the wind generating area. The selection of data collection technique is one of the important factors to

produce a 3D map. Data that can be transferred into the digital format are very important for acquiring spatial information of the earth surface. There are a variety of methods nowadays to obtain spatial data stored in databases such as GIS, remote sensing, LIDAR, laser scanning, conventional surveying, and aerial photogrammetric survey [9]. This research is focused on the use of photogrammetry method to produce 3D model maps of the earth surface using images. Aerial photographs are commonly taken using a metric aerial camera. Aerial views can provide high quality images for mapping purposes [10–12]. The metric camera is equipped with known point coordinates (known as Fiducial Mark) which are used as a reference in measuring the dimensions of an object. The metric camera is used for manned aircraft while nonmetric camera is used for image capturing, especially for small aircraft or Unmanned Aerial Vehicles (UAV).

The identification of coastal zones and coastlines is important in spatial data acquisition for coastal morphology study. UAV provides high resolution digital surface model and orthophoto products which are able to assist scientists in monitoring the morphology changes of coastline. The 3D representations can supply various types of information such as berm zones, erosion crest, and sand dunes. The structure from motion software is able to speed up the UAV photogrammetric processing with high spatial resolution, especially for coastal change studies which require accurate 3D visualizations of complex topography at the beach zones [13].

There are various types of UAVs available in the open market. The two main ones are fixed wing and multirotor. The most common type of multirotor UAV is Quad-copter and Hexa-copter. The cost of satellite images is expensive and gives the UAV mapping technology the opportunity as an alternative to save the cost of data acquisition in photogrammetry mapping. Aerial Photogrammetry can produce several products such as orthophotos, point cloud (3D distribution point), and DSM (digital surface model). The increasing use of UAVs for photogrammetry in aerial surveys has been drastic. UAVs are relatively inexpensive and many organizations have their own fleet, allowing for rapid surveys over large land areas where required [14, 15]. With GPS mounted drones, digital cameras, and powerful computers, surveys are done with an accuracy down to the centimeter level.

The use of UAVs in the mapping field has become increasingly popular today, especially since UAVs are now mounted with various types of sensors, including those in the field of remote sensing, photogrammetry, and land surveying. UAV's current capabilities in the considerable distance and the autopilot feature have facilitated the mapping work. Moreover, the aircraft movement nowadays is controlled by the Global Positioning System (GPS) and each position has a coordinate [16]. Data obtained from aerial photographs of UAV's camera are more stable in the presence of additional components such as the axis gimbal holder, making the picture more vertical and orthogonal from the earth. Therefore, images that have fewer oblique rates are made easier to process as the production of 3-dimensional model, point clouds, and Digital Terrain Model [11, 17].

Survey work includes the production of topographic maps, measurement of land area, monitoring of natural disasters such as landslides, coastal erosion, flood, and earthquakes, and estimation of the costs of losses involving property of the public. There are a lot of software tools nowadays that could be used in photogrammetry processing such as Agisoft and Pix4D. The leveling and GPS observation methods are time consuming and costly compared to UAV photogrammetry. GPS observation is simple and is highly dependent on satellite signals to determine the accuracy of the coordinates which are sent to the receiver [18]. If the signal is not satisfactory, then the accuracy of the coordinates given is large and out of tolerance.

Furthermore, the distribution of coordinate points on the surface area of the beach is much less compared to the cloud point with coordinate points x, y, z, which have a more extensive distribution. This study is based on the discretion and consultation with the different parties engaged in the mapping field. The aim of this study is to produce a surf zone 3D surface mapping by using a multirotor UAV.

Figure 1: Study area at Pantai Tanjung Gelam, Terengganu.

2. Materials and Methods

In this study, the selected area is the east coast of peninsular Malaysia. The east coast has a wide stretch of sand structure, especially in the state of Terengganu. In recent years, geomorphological processes have resulted in structural changes in the surf zone of uncertainty. The selected location is Pantai Pengkalan Maras which is located 10 km from the city of Kuala Terengganu (Figure 1).

This beach has fishing villages and picnic areas for the local population. The beach area is wide and safe for swimming activities. This beach is located in Mukim Batu Rakit whose majority of the local population are fishermen. The study area is located at $5^\circ\ 25'\ 7.55''$ latitude and $103^\circ\ 5'\ 00.73''$ longitude. This beach also has a coastal erosion effect by the adjacent beach known as Mengabang Telipot Beach. Therefore, this study area is suitable to see the changes on the coastal surface and surf zone changes pattern. This study can predict safe surf zone mapping for leisure activities on the selected beach. The research methodology of this study is as illustrated in Figure 2.

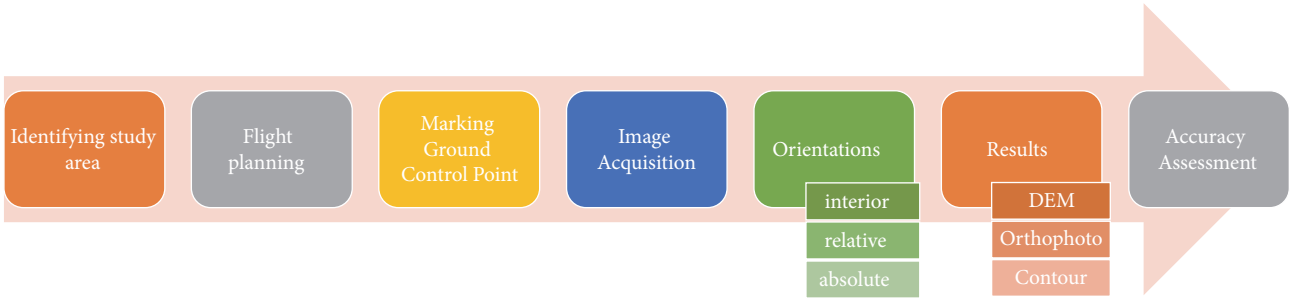

Figure 2: Research methodology.

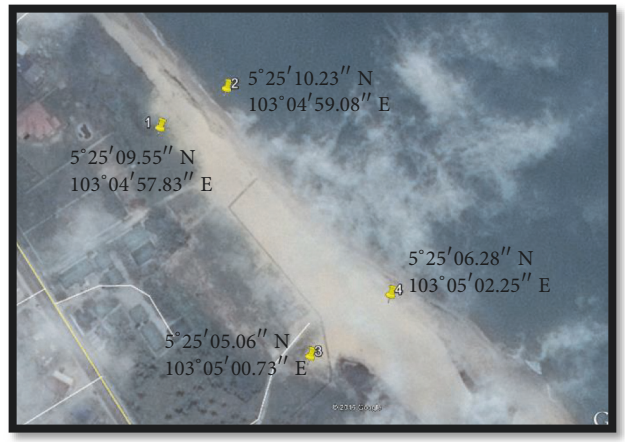

Figure 3: Four coordinates at study area.

Figure 4: Premark for GCPs and VPs.

This study used multirotor UAV known as DJI phantom 3 standard to acquire images at the study area. This UAV is commonly used for mapping purposes and easy to manoeuvre during flight mission. This UAV is equipped with Global Positioning System (GPS) which allows it to return at the hovering point when any emergency happens such as signal loss or battery weak. The specification of DJI phantom 3 standard is illustrated in Table 1.

UAV was integrated with GPS autopilot systems to manoeuvre the aircraft to the designed flight planning. The flight planning was designed using a smartphone app which is known as Altizure. The flight planning was based on Google satellite images in the app. UAV photogrammetry mapping has become easier with the assistance of intelligent apps. This app considers all parameters including altitude, overlap percentage, side lap percentage, camera angle, and speed. The user needs to determine the boundary of the study area using four coordinates at the corner to become an input in the apps. Coordinates for every corner are important to ensure the entire study area was covered. Once the surface area has been identified based on the four corners, flight planning can be designed as illustrated in Figure 3.

The photogrammetric flight planning starts from these four coordinates, and the number of images can be calculated based on specific camera parameters. The important parameters in flight planning calculation are dimension of study area, flying height or altitude, focal length, size of image, percentage of overlap and sidelap. The parameters used in this study are illustrated in Table 2.

There are two types of control point marking, namely, postmarking and premarking. Postmarking means the selection of control points after flight mission while premarking means the selection of control point before flight mission. Therefore, in this study premarking has been applied due to the condition of study area. The study area has difficulty in identifying any object to become premark; therefore the man-made premarkings were required. Figure 4 shows the premark design in X shape used in this study.

Table 1: The aircraft and sensor specification (dji.com 2016).

Category	Specification
Weight (including battery and propellers)	1216 g
Diagonal size (excluding propellers)	350 mm
Max ascent speed	5 m/s
Max descent speed	3 m/s
Max speed	16 m/s (atti mode, no wind)
Max service ceiling above sea level	6000 m (default altitude limit: 120 m above take off point)
Max flight time	Approx. 25 minutes
Operating temperature	0°c to 40°c
GPS mode	Built-in gps
Camera Sensor	
Sensor	1/2.3" Effective pixels: 12 M
Lens	FOV (Field of View) 94° 20 mm (35 mm format equivalent) f/2.8
ISO Range	100-3200 (video) 100-1600 (photo)
Shutter Speed	8s -1/8000s
Image Max Size	4000×3000
Still Photography Modes	Single Shot Burst Shooting: 3/5/7 shots Auto Exposure Bracketing (AEB): 3/5 Bracketed Frames at 0.7EV Bias Time-lapse
Video Recording Modes	2.7K: 2704 x1520p 24/25/30 (29.97) FHD: 1920x1080p 24/25/30 HD: 1280x720p 24/25/30/48/50/60
Max Video Bitrate	40 Mbps
Supported File Formats	FAT32 (≤ 32 GB); exFAT (> 32 GB)
Supported SD Card Types	Micro SD Card 8 GB included
Operating Temperature	32° to 104° F (0° to 40° C)
Photo	JPEG, DNG
Video	MP4, MOV (MPEG-4 AVC/H.264)

Table 2: Flight planning parameters.

Parameter	Characteristic
Flight Altitude	50 meter
Front lap	85%
Side lap	75%
Flight Time	6 min 24s
Focal Length	3.6mm
Image Size	4000×3000
Area cover	16920 m^2
Total Image	125
Flight speed/velocity	2 m/s

The size of man-made premark is dependent on the ground sampling distance. The ground sampling distance can be calculated using pixel size of the image and scale. The ground sampling distance in this study is about 2.2cm where the A4 paper with X cross can be used as premark in this study. The premark must can be seen in the aerial images and is not too small because it can create an ambiguity during absolute orientation. Therefore, 13 premarks have been created before flight mission where four represent Ground Control Points (GCPs) and nine represent verification points (VPs). After all, GCPs and VPs have been marked; then the flight mission can be performed. This study used Altizure app to create flight mission at the study area. Altizure app is one of the free apps available in the market. This app can allow UAV to perform autonomous flight mission starting from hovering until landing. The autonomous flight mission can be performed using GPS autopilot system which can navigate the UAV fly at the designed waypoints or flight lines. The autonomous flight mission provides Google satellite images as a basemap for flight mission. The interface of Altizure as illustrated in Figure 5.

Table 3: GCPs and VPs coordinates.

Points	Easting (m)	Northing (m)	Height (m)
GCP1	601024.967	563532.623	2.86755
GCP2	601059.511	563574.423	0.79005
GCP3	601163.523	563383.713	2.3648
GCP4	601206.158	563429.031	0.67485
VP1	601104.386	563533.006	4.561
VP2	601106.665	563545.727	4.090
VP3	601152.647	563476.592	6.932
VP4	601285.502	563420.733	0.606
VP5	601235.526	563466.267	4.054
VP6	601182.458	563520.691	4.514
VP7	601159.985	563506.212	7.209
VP8	601219.335	563447.876	6.034
VP9	601188.368	563477.391	6.334

The study area has a dimension of approximately 235m x 72m. However, photogrammetric method requires capturing images outside this dimension to make sure all images have stereomodels. The Altizure app is very friendly; the user only needs to select the specific parameters and the app will automatically calculate the time of flight mission, number of strips, and number of photos to cover the whole study area. After the flight mission was performed, the acquired images were downloaded to a personal computer. The user needs to check the quality of acquired images to make sure they are free from blur and distortion.

After flight mission, the user must confirm all GCPs and VPs exist in the acquired images. In this study, four GCPs were used as a control for image processing while nine VPs were used to check the accuracy of photogrammetric products. Each control point must exist in at least two pairs of images in order to fulfill photogrammetric method. All GCPs and VPs coordinates were observed using Real Time Kinematic (RTK) GPS observations. The distribution of GCPs and VPs is illustrated in Figure 6, and the coordinates of each GCP and VP are shown in Table 3.

Figure 5: Flight path on flight planning.

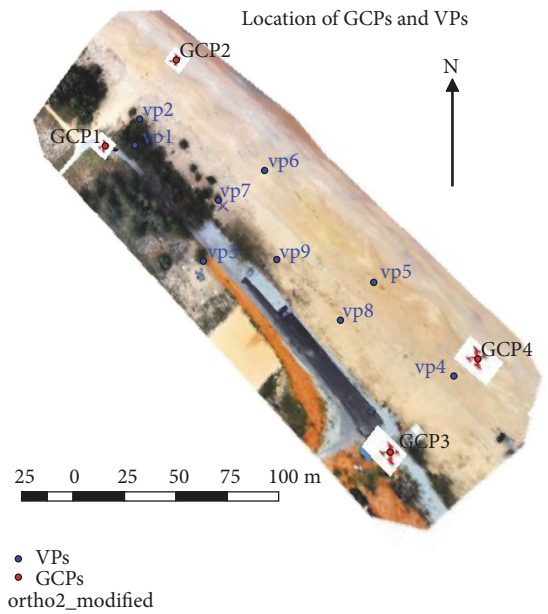

Figure 6: The location of GCPs and VPs.

GCPs were used as the controls for image processing and VPs were used to assess the accuracy of the photogrammetric products. Each GCP must appear in at least two overlapping images which are also known as the stereomodel. The method used to observe the GCP utilizes Topcon GPS with RTK. The observations took about 20 minutes per point.

After all GCPs and VPs have been observed and obtained their coordinates, the image processing can proceed. The photogrammetric method requires that the acquired images go through interior, relative, and absolute orientations. The commercial software Pix4D was used to process the UAV images and produce all photogrammetric products. Pix4D software has classified the processing stage into three; namely, phase one is initial processing, phase two is point cloud and mesh, and phase three is DSM and orthomosaic. The processing parameters based on the three main stages are illustrated in Figure 7.

The initial processing stage requires user to choose keypoints image scale, and this study used full keypoints image scale, which means the matching used original image scale and selected tie point measurement throughout the full image pairs. The alignment of images is also based on the initial

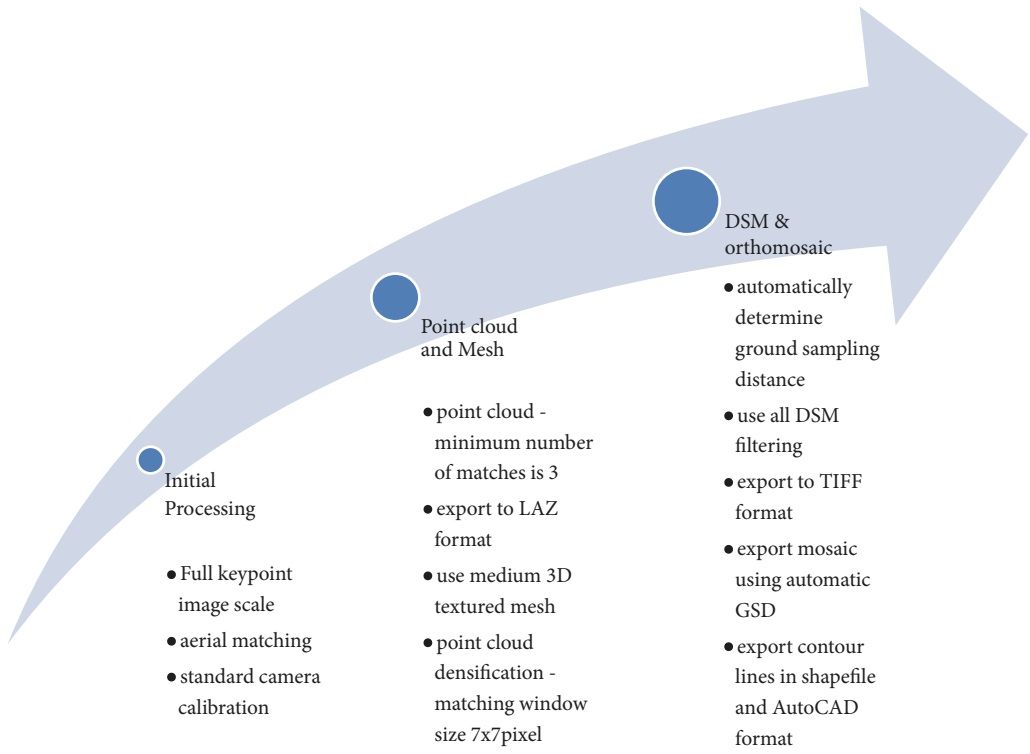

Figure 7: Pix4D image processing stages.

GPS coordinates which have been geotagged at the centre of each image. The standard camera calibration was performed automatically during initial processing based on the acquired images. The internal camera parameters were directly applied during image processing. The image matching for all image pairs has been done automatically in this software.

The point cloud and mesh stage requires user to set the point cloud densification. This study uses half image size for image scale, uses optimal size for point density, and sets at least 3 points as the minimum number of matches. The 3D textured mesh setting used medium resolution in this study due to the limitation of personal computers which are unable to perform high resolution setting. The point cloud densification uses 7x7 matching window size.

This software performed the tie point measurement automatically. Tie points contained x, y, and z coordinates based on the stereomodel at the study area. The point cloud data represented thousands to millions of tie points and it showed the 3D surface which represented the earth surface. The point cloud can be divided into two conditions, i.e., true color with texture or false color based on height value (Figure 8).

The DSM and orthomosaic stage require user to choose the resolution for DSM and orthomosaic. This study chooses the automatic calculated GSD and uses automatic noise filtering and surface smoothing for DSM. The raster DSM and orthomosaic were exported to GeoTIFF format. The contour lines generated from DTM were exported to shapefile and AutoCAD format.

3. Results and Discussion

In this study, several photogrammetric products were produced to support surf zone mapping such as DEM, orthophoto, and contour (Figure 9). Digital elevation model is one of the final products before orthophoto. DEM is digital model data indicating the height of surface in the data model. The DEM is in the GeoTIFF format and can be opened using the ArcGIS software. In this study, ArcGIS is a medium to view DEM and orthophoto. The orthophoto is the final product in the photogrammetry process. The DEM was used as an input to generate orthophoto. Orthophoto is the product that is free from any distortion and relief which has been corrected using DEM. The contour data were generated from DEM using the ArcGIS software. The contour interval of 0.5 m was used for the surf zone mapping. The interval could determine the changes of surf zone at different epochs. The contour lines were superimposed with the orthophoto to determine the changes of the surf zone.

The verification points were analyzed using the root mean square error (RMSE). The RMSE is used to measure the accuracy of the photogrammetric results which is based on actual and measured data. The calculation of RMSE for northing, easting, and height is illustrated in Tables 4 and 5.

In this study, it was found that the accuracy of northing coordinates is about one meter while that of easting coordinates is about 0.8m, and height coordinates recorded an accuracy of about 0.4m. Therefore, the accuracy of planimetric coordinates is about 1.3m. Therefore, the height

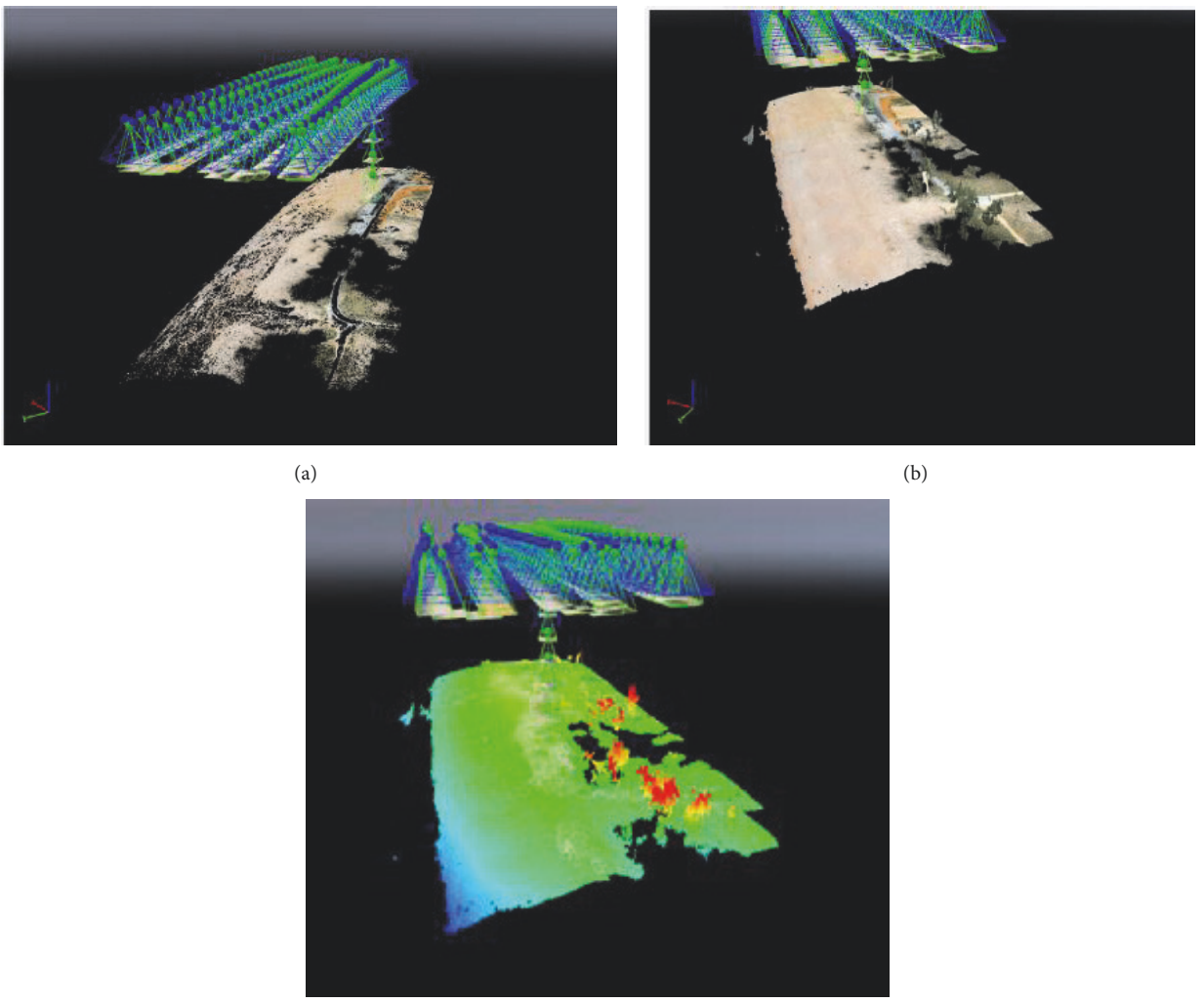

(a) (b)

(c)

Figure 8: Point cloud: (a) sparse point cloud, (b) true color, and (c) false color.

Table 4: Error and root mean square error for northing and easting.

VP	N(m)	N'(m)	Error (m)	E(m)	E'(m)	Error (m)
1	563533.006	563531.800	1.206	601039.386	601038.570	0.816
2	563545.727	563544.770	0.957	601041.665	601040.420	1.245
3	563476.592	563477.830	-1.238	601072.647	601073.310	-0.663
4	563420.733	563419.590	1.143	601194.502	601193.830	0.672
5	563466.267	563466.790	-0.523	601155.526	601154.290	1.236
6	563520.691	563519.810	0.881	601102.458	601101.900	0.558
7	563506.212	563505.530	0.682	601079.985	601079.360	0.625
8	563447.876	563447.110	0.766	601139.335	601140.320	-0.985
9	563477.391	563478.860	-1.469	601108.368	601108.250	0.118
	RMSE-N	$\sqrt{\frac{\sum (N - N')^2}{n}}$	**1.026**	**RMSE-E**	$\sqrt{\frac{\sum (E - E')^2}{n}}$	**0.838**

$*n$: number of points.

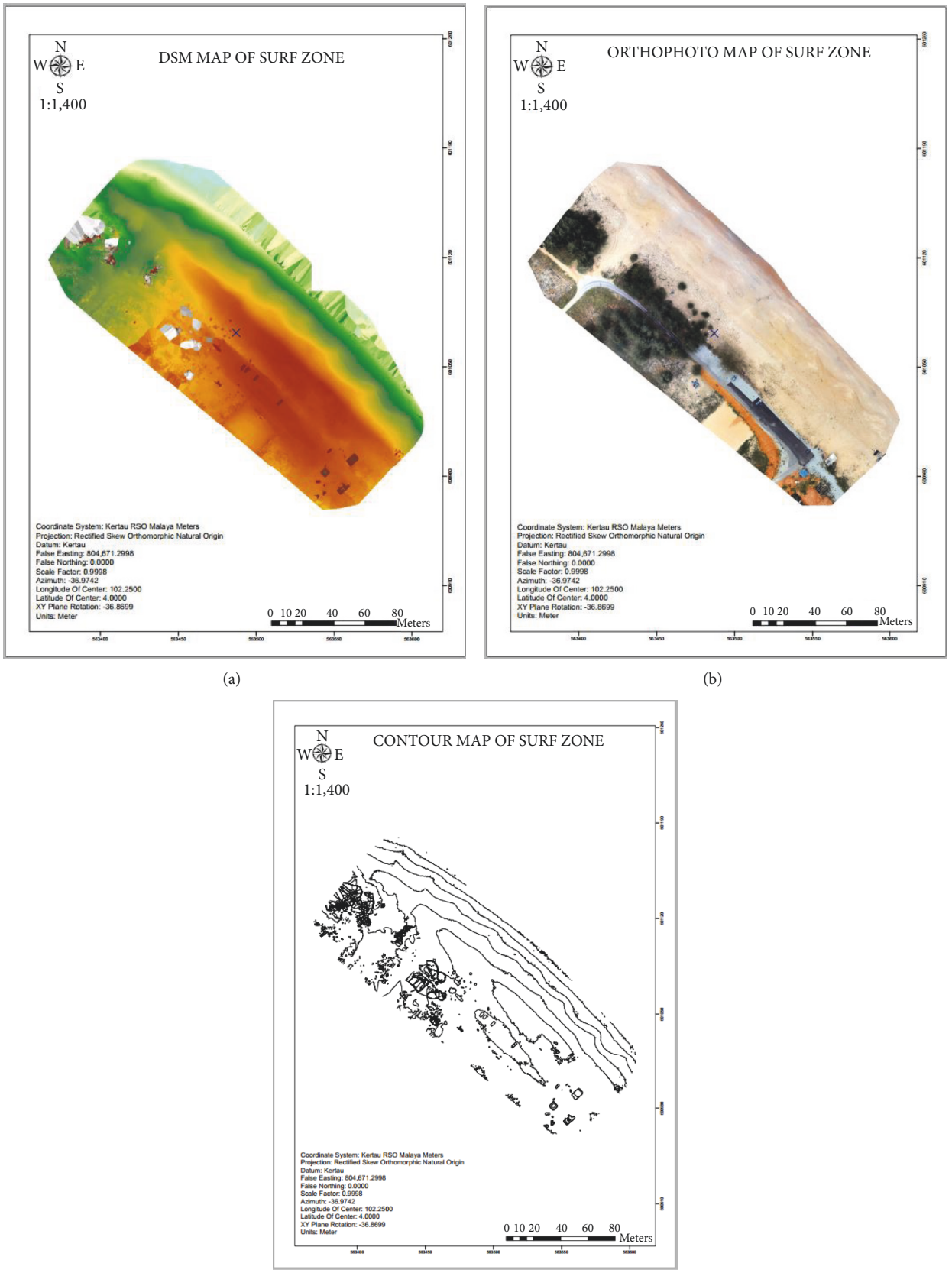

Figure 9: Results: (a) DEM, (b) orthophoto, and (c) contour.

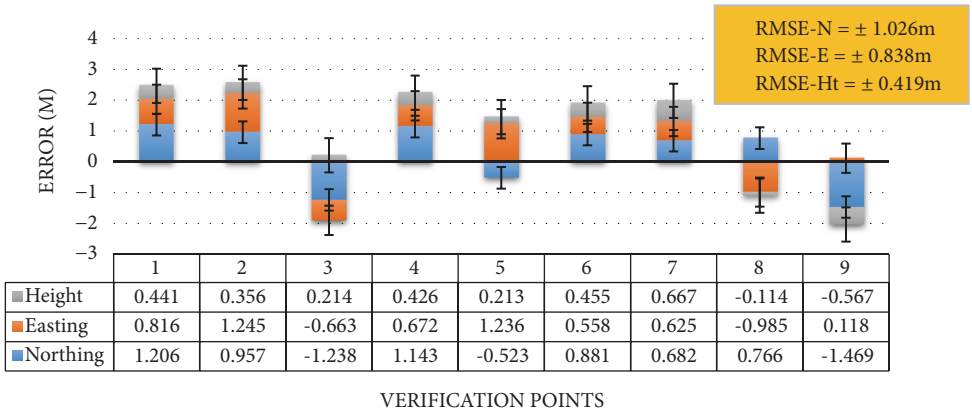

	1	2	3	4	5	6	7	8	9
Height	0.441	0.356	0.214	0.426	0.213	0.455	0.667	-0.114	-0.567
Easting	0.816	1.245	-0.663	0.672	1.236	0.558	0.625	-0.985	0.118
Northing	1.206	0.957	-1.238	1.143	-0.523	0.881	0.682	0.766	-1.469

Figure 10: Error and RMSE results for northing, easting, and height coordinates.

Table 5: Error and root mean square error for height coordinates.

Ht(m)	Ht'(m)	Error (m)
7.361	6.920	0.441
6.890	6.534	0.356
9.732	9.518	0.214
3.406	2.980	0.426
6.854	6.641	0.213
7.314	6.859	0.455
10.009	9.342	0.667
8.834	8.948	-0.114
9.134	9.701	-0.567
RMSE-Ht	$\sqrt{\frac{\sum (Ht - Ht')^2}{n}}$	**0.419**

∗n: number of points.

coordinates provide better accuracy compared to planimetric coordinates. These results are due to the condition of study area where the surface of study area is covered by sand or coastal area. The study area does not have small vegetation growth which can affect the development of DEM. The planimetric coordinates recorded an accuracy of more than one meter due to the difficulty in matching the sand at the study area by the image matching algorithm. The image matching algorithm needs an obvious texture to identify the same features or object in a stereopair, which is hard to find at this study area. Therefore, the accuracy of planimetric coordinates is more than a meter.

The RMSE is used to determine the level of accuracy for the surf mapping results. The RMSE was calculated based on the actual and measured coordinates for northing, easting, and height coordinates. The error for each verification point is shown in Figure 10.

Based on Figure 10, the northing and easting coordinates recorded RMSE at about 1.026m and 0.838m with the height coordinate at about 0.419m. Based on this result, the planimetric coordinates of surf map have about one meter accuracy while the height has about half a meter. The changes of surf mapping zone can only be detected if the changes are more than two centimeters. The changes below this value cannot be analyzed. However, the accuracy of the surf zone mapping from 50m altitudes can only achieve approximately one meter and half a meter for planimetric and height coordinates, respectively.

The regression is to estimate the unknown effect of changing one variable over another (Stock and Watson, 2003). The linear regression is a statistical method to summarize and study relationships between two continuous (quantitative) variables. Figure 11 illustrates the linear regression graph for northing, easting, and height.

Figure 11 shows the relationship between actual and measured coordinates for northing, easting, and height, also analyzed using a linear regression graph. The northing coordinates recorded 99.9%, easting coordinates were 99.9%, and height coordinates were 97.2%. Hence, in this study the relationship between two variables, measured and actual, showed a strong relationship which is above 97% for easting, northing, and height. Therefore, this study can be accepted for surf zone mapping studies. This study also used a profile graph for surf zone mapping to determine the coastal changes at different epochs. This study used 20 changes to study the pattern of the surf zone (Figure 12). The longitudinal and cross section profile graph can record the earth surface profile at the surf zone mapping. The profile graph is very important for the disaster management team to carry out the prevention steps at the risky surf zone.

The triangulated irregular network is used in this study to model the pattern changes of 3D surf mapping zone in different months. This study chose four different months, i.e., July, September, November, and January, for the sake of combining normal and monsoon seasons. Therefore, the 3D surf zone mapping is totally different from July to January where the changes of surf zone mapping were affected due to the normal and monsoon seasons (Figure 13).

Based on Figure 13, the triangulated irregular network at normal season shows that the classification of terrain model is less than 3m, with the surf zone being quite flat during normal season. The changes of terrain can be obviously seen in September using triangulated irregular network. The classification of terrain model in September covered seven classes, with the maximum range of terrain being about 9-11m.

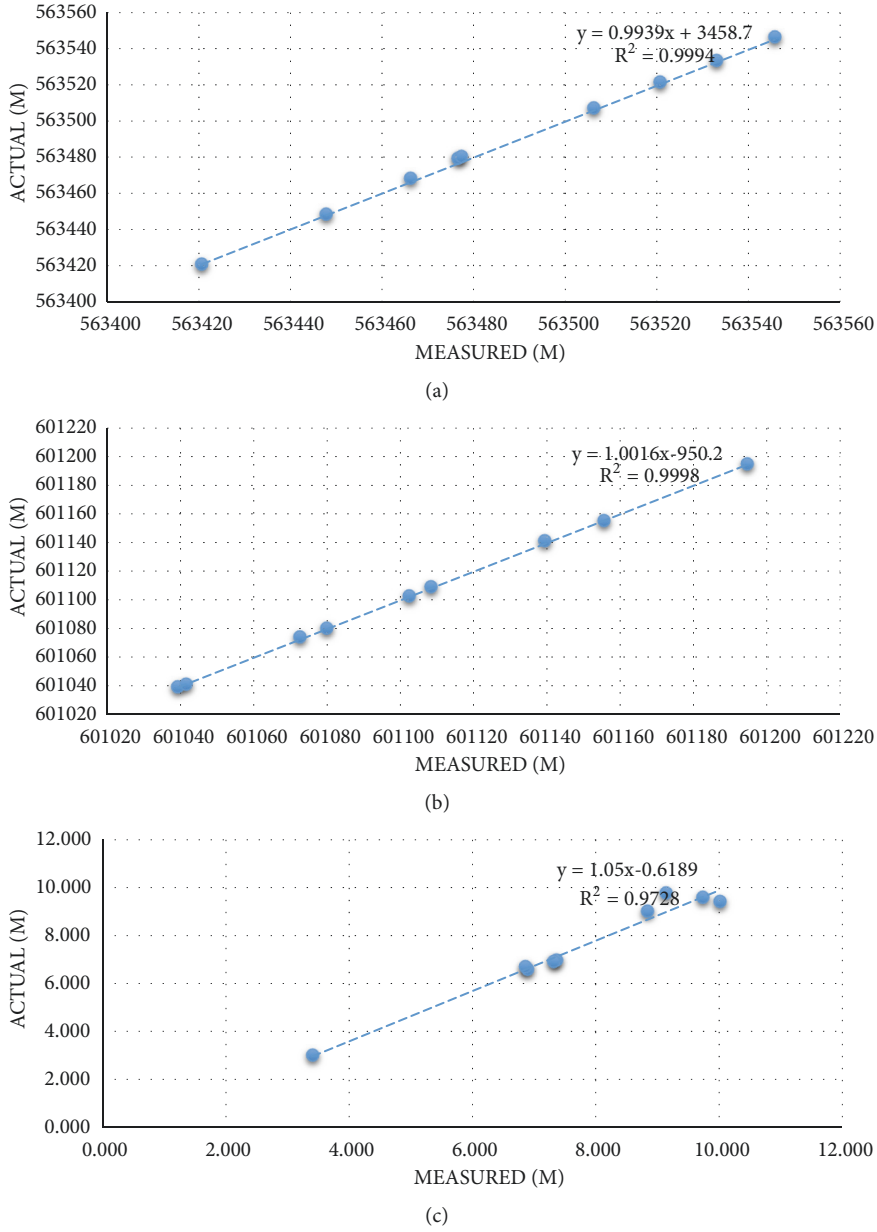

Figure 11: Linear regression: (a) X coordinate, (b) Y coordinate, and (c) Z coordinate.

During November, the terrain model covered five classes where the maximum elevation is about 5-7m. during January, the terrain model covered four classes where the maximum elevation is about 3-5m. UAV is very practical for surf zone mapping and it can be used for disaster management for long-term studies.

This study also investigates the cost, time, and labor need for the surf zone mapping. Table 6 illustrates the details of cost, time, and labor used to produce surf zone mapping using UAV and conventional methods. Based on Table 6, the total cost, the time spent for image acquisition and image processing, and labor needed for UAV are less than those in conventional methods. However, the most important issue is that the UAV could provide rapid data acquisition and results for the fast decision making. This detail is based on the study area of 16920m^2. UAV could offer more advantages for larger study areas.

4. Conclusion

In this study, it can be concluded that the UAV is able to model the changes of surf zone mapping at the coastal area. The accuracy of photogrammetric results for 3D surf zone mapping for northing coordinate is 1.026m, for easting coordinate is 0.838, and for height coordinate is 0.419. The planimetric coordinates have more errors compared to height coordinates due to the condition of study area where the surface is covered by sand. The image matching requires the

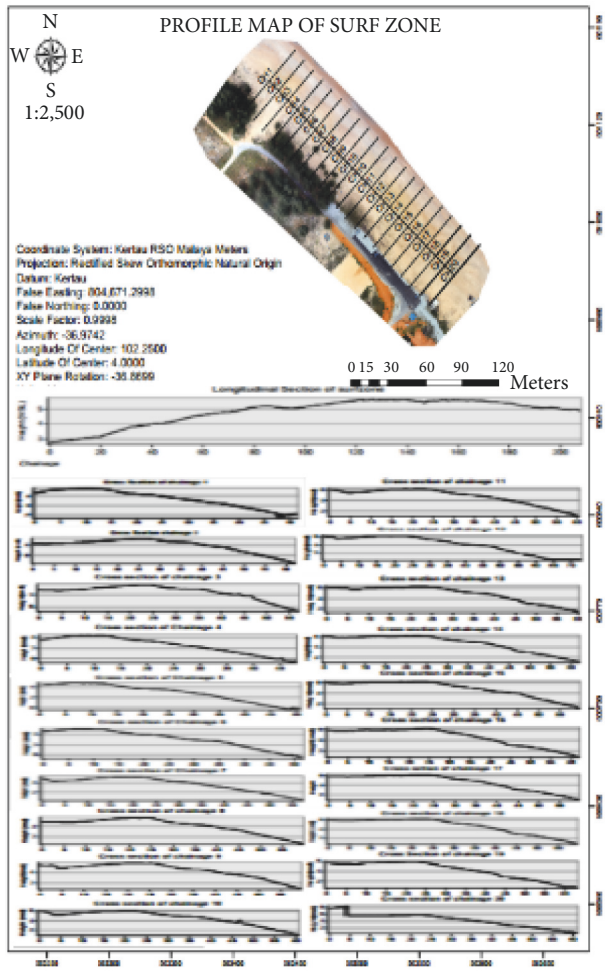

Figure 12: Profile graph.

Table 6: The details of cost, time, and labour needed for UAV and conventional methods.

	UAV	Conventional
Instrument	UAV multirotor (($600)	Total Station ($8500)
Positioning System (GCPs)	Topcon hyper ($5790)	-
Processing Software	Pix4D ($495)	CDS ($200)
Time	Data Capture – 6min 24s Data processing – 30min (computer specifications- i7, 16GB RAM)	Traversing/tacheometry work – 2 hours Data processing – 30min
Labour	1 person	3 people
Total (instruments, processing software, time and labour	Cost - $6885 Time – 36min 24s Labour – 1 Person	Cost - $8700 Time – 2 hours and 30min Labour – 3 persons

different texture to identify the same feature or object on stereopair, but in this case the software struggles to identify the same features on stereopair because the texture of sand looks almost similar. Therefore, the planimetric coordinates accuracy is less than that of the height coordinates. This study also proved that the changes of surf mapping zone during normal and monsoon season can be identified using profile graph and triangulated irregular network produced by UAV. The UAV might have some difficulties in dealing with the wind as it can influence the accuracy of surf zone mapping. Therefore, careful planning during image acquisition is a crucial part in any photogrammetric mapping. It is recommended that the number of GCPs should be increased to improve results accuracy for future studies.

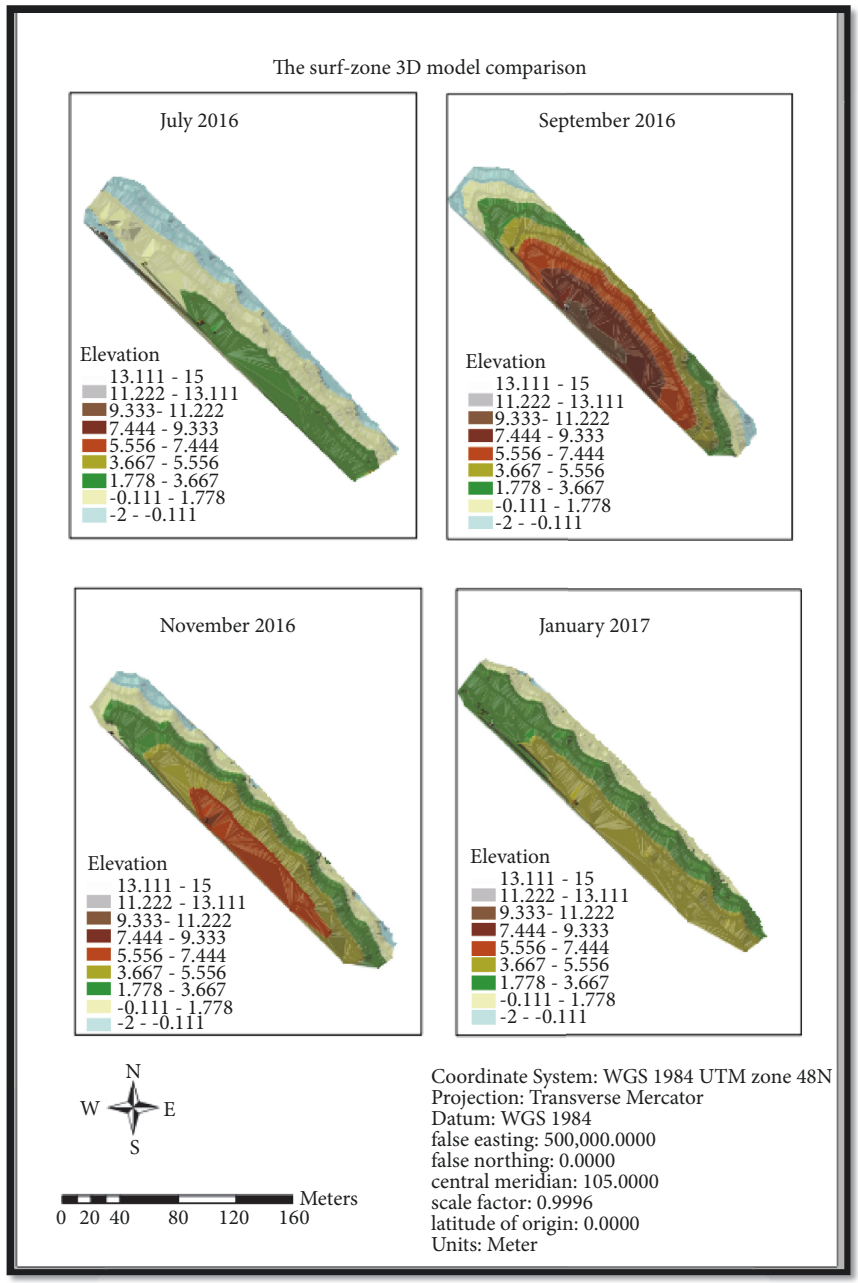

Figure 13: Triangulated irregular network for surf mapping zone.

Data Availability

The data used to support the findings of this study are available from the corresponding author upon request.

Conflicts of Interest

The authors declare that they have no conflicts of interest.

Acknowledgments

Faculty of Architecture, Planning, and Surveying Universiti Teknologi MARA (UiTM), Research Management Institute (RMI), and Ministry of Higher Education (MOHE) are greatly acknowledged for providing the fund BESTARI 600-IRMI/MyRA 5/3/BESTARI (001/2017) to enable this research to be carried out. The authors would also like to thank the people who were directly or indirectly involved in this research.

References

[1] L. J. Moore, "Shoreline mapping techniques," *Journal of Coastal Research*, vol. 16, no. 1, 2000.

[2] R. Hashim and Z. A. Latif, "Langkawi's sustainable regeneration strategy and natural heritage preservation," *EnvironmentAsia*, vol. 8, no. 2, pp. 1–8, 2015.

[3] J. C. Brock and S. J. Purkis, "The emerging role of lidar remote sensing in coastal research and resource management," *Journal of Coastal Research*, pp. 10–2112, 2009.

[4] C. D. Drummond, M. D. Harley, I. L. Turner, A. N. A. Matheen, and W. C. Glamore, "UAV applications to coastal engineering," in *Proceedings of the Australian Coasts and Ports 2015 Conference*, pp. 267–272, New Zealand, September 2015.

[5] N. A. Adnan, P. M. Atkinson, Z. M. Yusoff, and A. R. A. Rasam, "Climate variability and anthropogenic impacts on a semi-distributed monsoon catchment runoff simulations," in *Proceedings of the 2014 IEEE 10th International Colloquium on Signal Processing and Its Applications, CSPA 2014*, pp. 178–183, Malaysia, March 2014.

[6] I. L. Turner, M. D. Harley, and C. D. Drummond, "UAVs for coastal surveying," *Coastal Engineering*, 2016.

[7] J. Anderson, "On trend and on the wave: carving cultural identity through active surf dress," *Annals of Leisure Research*, vol. 19, no. 2, pp. 212–234, 2016.

[8] A. R. Vetrella, G. Fasano, and D. Accardo, "Cooperative navigation in GPS-challenging environments exploiting position broadcast and vision-based tracking," in *Proceedings of the 2016 International Conference on Unmanned Aircraft Systems, ICUAS 2016*, pp. 447–456, USA, June 2016.

[9] J. Vrbancich, W. Lieff, and J. Hacker, "Demonstration of two portable scanning LiDAR systems flown at low-altitude for investigating coastal sea surface topography," *Remote Sensing*, vol. 3, no. 9, pp. 1983–2001, 2011.

[10] K. G. Nikolakopoulos, K. Soura, I. K. Koukouvelas, and N. G. Argyropoulos, "UAV vs classical aerial photogrammetry for archaeological studies," *Journal of Archaeological Science: Reports*, 2017.

[11] A. Papakonstantinou, K. Topouzelis, and G. Pavlogeorgatos, "Coastline zones identification and 3D coastal mapping using UAV spatial data," *ISPRS International Journal of Geo-Information*, vol. 5, no. 6, p. 75, 2016.

[12] K. N. Tahar, "Aerial terrain mapping using unmanned aerial vehicle approach," in *Proceedings of the 22nd Congress of the International Society for Photogrammetry and Remote Sensing, ISPRS 2012*, vol. 39, pp. 493–498, Australia, September 2012.

[13] J. A. Gonçalves and R. Henriques, "UAV photogrammetry for topographic monitoring of coastal areas," *ISPRS Journal of Photogrammetry and Remote Sensing*, vol. 104, pp. 101–111, 2015.

[14] H. El-Sallabi, A. Aldosari, and S. Alkaabi, "UAV path planning in absence of GPS signals," in *Proceedings of the Unmanned Systems Technology XIX*, R. E. Karlsen, D. W. Gage, C. M. Shoemaker, and H. G. Nguyen, Eds., vol. 10195, p. 1019516, International Society for Optics and Photonics, Anaheim, Ca, USA, 2017.

[15] K. A. Hashim, A. Ahmad, A. M. Samad, K. NizamTahar, and W. S. Udin, "Integration of low altitude aerial & terrestrial photogrammetry data in 3D heritage building modeling," in *Proceedings of the 2012 IEEE Control and System Graduate Research Colloquium, ICSGRC 2012*, pp. 225–230, Malaysia, July 2012.

[16] S. A. H. Sulaiman, K. H. Talib, M. A. M. Wazir, and O. M. Yusof, "Evaluation of geoid height derived by geopotential model and existing regional geoid model," in *Proceedings of the 2013 IEEE 9th International Colloquium on Signal Processing and Its Applications, CSPA 2013*, pp. 106–110, March 2013.

[17] X. Meng, N. Shang, X. Zhang et al., "Photogrammetric UAV mapping of terrain under dense coastal vegetation: An object-oriented classification ensemble algorithm for classification and terrain correction," *Remote Sensing*, vol. 9, no. 11, article no. 1187, 2017.

[18] K. N. Tahar, "Efficiency and cost comparison of UAV/Field survey," in *Proceedings of the 2015 International Conference on Space Science and Communication (IconSpace)*, pp. 428–433, Langkawi, Malaysia, August 2015.